Atmospheric Correction of Landsat ETM+ Land Surface Imagery—Part I: Methods

Shunlin Liang, *Senior Member, IEEE*, Hongliang Fang, and Mingzhen Chen

***Abstract*—To extract quantitative information from the Enhanced Thematic Mapper-Plus (ETM+) imagery accurately, atmospheric correction is a necessary step. After reviewing historical development of atmospheric correction of Landsat thematic mapper (TM) imagery, we present a new algorithm that can effectively estimate the spatial distribution of atmospheric aerosols and retrieve surface reflectance from ETM+ imagery under general atmospheric and surface conditions. This algorithm is therefore suitable for operational applications. A new formula that accounts for adjacency effects is also presented. Several examples are given to demonstrate that this new algorithm works very well under a variety of atmospheric and surface conditions. The companion paper will validate this method using ground measurements, and illustrate the improvements of several applications due to atmospheric correction.**

***Index Terms*—Adjacency effect, aerosol, atmospheric correction, land surface, reflectance.**

I. Introduction

LANDSAT thematic mapper (TM) imagery have been extensively used for agricultural evaluation, forest management inventories, geological surveys, water resource estimates, coastal zone appraisals, and a host of other applications. The Enhanced Thematic Mapper-Plus (ETM+) on Landsat7 that was launched on April 15, 1999 is providing observations at a higher spatial resolution and with greater measurement precision than the previous TM [16]. As the utility of these data becomes more quantitative, the accurate retrieval of surface reflectance becomes increasingly important. For example, almost all of the canopy radiative transfer models that are used for inverting land surface biophysical parameters are based on surface reflectance.

Unfortunately, a very large percentage of imagery are severely contaminated by aerosols, clouds, and cloud shadows. TM images can be potentially more useful if we can remove the effects of aerosols, thin clouds, and cloud shadows. This procedure for retrieving surface reflectance is usually called atmospheric correction.

Atmospheric correction consists of two major steps: parameter estimation and surface reflectance retrieval. As long as all atmospheric parameters are known, retrieval of surface reflectance is relatively straightforward when the surface is assumed to be Lambertian for TM-type data. Earlier studies attempt to develop approximate solutions to the atmospheric radiative transfer equation for quick calculations, but the typical approach that now has been widely accepted is the so-called look-up table method [12]. With this approach, radiative transfer codes are used off-line to compute tables for on-line corrections. So then, the estimation of atmospheric parameters from the imagery itself is the most difficult and challenging step.

Atmospheric effects include molecular and aerosol scattering and absorption by gases, such as water vapor, ozone, oxygen and aerosols. Molecular scattering and absorption by ozone and oxygen are relatively easy to correct because their concentrations are quite stable over both time and space. The effect of water vapor absorption is significant for the TM/ETM+'s near-infrared (IR) channels, but there is insufficient information that allows us to estimate water vapor content from TM/ETM+ imagery. The practical approach is to use climatology data or other satellite products. The most difficult component of atmospheric correction is to eliminate the effect of aerosols. The fact that most aerosols are often distributed heterogeneously makes this task more difficult.

After reviewing the historical development of atmospheric correction, we will present a new algorithm that is designed to handle general atmosphere and surface conditions and is therefore suitable for operational applications. The key feature of this new algorithm is the automatic estimation of heterogeneous aerosol distribution from the imagery itself. Because of the high spatial resolution, the surface adjacency effect is considerable for a general landscape where surface reflectance is not homogeneous. This has also been considered in this study.

II. Review of the Existing Atmospheric Correction Algorithms

There is a relatively long history of the quantitative atmospheric correction of TM imagery. All methods reported in the literature can be roughly classified into the following groups: invariant-object, histogram matching, dark object, and the contrast reduction. It is not our intention to review each algorithm conclusively, but it will be helpful to understand the advantages and limitations of representative algorithms. Each group will be briefly evaluated in the following sections. Note that most statistical methods (e.g., [43], [38], [26]) and the methods that do not correct heterogeneous aerosol scattering are not discussed here.

A. Invariant-Object Methods

The Invariant-Object method assumes that there are some pixels in any given scene whose reflectances are quite stable.

Manuscript received September 29, 2000; revised August 20, 2001. This work was supported in part by the U.S. National Aeronautics and Space Administration (NASA), Washington, DC, under Grant NAG5-6459.

S. Liang, H. Fang, and M. Chen are with the Laboratory for Global Remote Sensing Studies, Department of Geography, University of Maryland, College Park, MD 20742 USA (e-mail: sliang@geog.umd.edu).

Publisher Item Identifier S 0196-2892(01)10989-7.

A linear relation for each band based on the reflectance of these "invariant objects" can be used to normalize images acquired at different times. This method was successfully used in the FIFE (first ISLSCP field experiments) TM imagery processing [17]. It is a relative normalization. If there are simultaneous ground reflectance measurements available or some assumptions about surface properties are made [35], [6], it can be an absolute correction procedure.

This method is simple and straightforward, but it is essentially a statistical method and performs only a relative correction. Another major limitation is its difficulty in correcting heterogeneous aerosol scattering.

B. Histogram Matching Methods

In the histogram matching method, it is assumed that the surface reflectance histograms of clear and hazy regions are the same. After identifying clear sectors, the histograms of hazy regions are shifted to match the histograms of their reference sectors (clear regions) [40], [41].

The idea behind this method is quite simple and it is also easy to implement. This method has been incorporated into ERDAS Imagine image processing software package. The PCI image processing software package is also based on a similar principle. However, the major assumption is not valid when the relative compositions of different objects and their spectral reflectances are different. This method also does not work well if the spatial distribution of aerosol loadings vary dramatically. If the scene is divided into many small segments to deal with the variable aerosol loadings, it is most likely that the major assumption of this method will be violated.

C. Dark-Object Methods

If a scene contains dense vegetation, ETM+/TM 7 band (around 2.1 μm) can be used to identify these dense vegetation pixels and their reflectances have strong correlations with band 1 (blue) and 3 (green) reflectances. Since dense vegetation has very low reflectance in the visible spectrum, they are referred to as "dark objects." This method has a long history [23], [48], [24], [22], [28], [37] and is probably the most popular atmospheric correction method. Both the moderate-resolution imaging spectroradiometer (MODIS) and medium resolution imaging spectrometer (MERIS) atmospheric correction algorithms [24],[42] are based on this principle. However, this method does not work well if the dense vegetation is not widely distributed over the hazy regions. The required existence of dense vegetation canopies is a serious limitation to many land surface imagery acquired over the winter season in the northern hemisphere. The empirical relations between band 7 reflectance and blue (band 1) and green (band 3) reflectances may also vary under different vegetation conditions.

D. Contrast Reduction Methods

For regions where surface reflectance are very stable, the variations of the satellite signal acquired at different times may be attributed to variations of the atmospheric optical properties. Aerosol scattering reduces variance of the local reflectance. The larger the aerosol loading, the smaller the local variance. Thus, the local variance can be used for estimating the aerosol optical depth. This method has been successfully applied to desert dust monitoring [45], [44]. Its assumption of invariant surface reflectance limits its global applications because under general conditions surface reflectance changes in both space and time.

III. The New Method

To overcome the problems associated with the existing methods discussed above, we have developed a new atmospheric correction algorithm in which the key component is to estimate the spatial distribution of aerosol loadings under general conditions, and to correct adjacency effects more effectively.

To calculate aerosol effects accurately, we need not only aerosol optical depth, but also single scattering albedo and the phase function. The last two variables can be determined from aerosol climatology data [18], which will be updated by EOS Terra products (e.g., MODIS and MISR-Multiangle Imaging SpectroRadiometer) soon. In the current version, the water vapor content is also determined from the climatology data. We should be able to determine it from other satellite products in the near future. MODIS is providing two products using both near-Infrared (IR) water absorption bands [14] and the differential sounding method [33] in the Terra platform and will continue in the Aqua platform. Atmospheric infrared sounder (AIRS) on Aqua will also provide an accurate total water vapor content product [3].

In the following, we will briefly describe the procedures for creating look-up tables, estimating aerosol optical depth, correcting surface adjacency effects, and retrieving surface reflectance.

A. Creation of the Look-up Tables

It is not practical to solve the atmospheric radiative transfer equation numerically for operational atmospheric correction. There have been many different approximate solutions to the atmospheric radiative transfer equation that enable us to calculate atmospheric quantities quickly, but their accuracies are limited. The alternative solution is the table look-up method in which different atmospheric quantities are calculated off-line and organized in the form of tables. These quantities can be determined on-line by searching the tables in the operational correction procedure. The basic procedure is similar to that used in our earlier study [28], a brief outline is provided here.

For a flat, Lambertian surface under a horizontally homogeneous atmosphere, the top-of-atmosphere (TOA) radiance can be expressed by the classic formula [29]

$$L(\mu_v) = L_p(\mu_v) + \frac{r}{1 - rS}\mu_s F_0 \gamma(\mu_s)\gamma(\mu_v) \tag{1}$$

where

- L_p path radiance;
- r surface reflectance;
- S spherical albedo of the atmosphere;
- πF_0 incident solar flux density perpendicular to the solar indent beam at the top of the atmosphere.

$\gamma(\mu)$ is the total transmittance from the surface to the sensor or sun. μ_s and μ_v are the cosine values of the solar and viewing

zenith angles, respectively. For ETM+/TM data, the viewing zenith angle is very small, so μ_v can be assumed to be one.

We need to create the tables for L_p, S, and $F(\mu_s F_0 \gamma(\mu_s)\gamma(\mu_v))$ at different solar zenith angles, aerosol optical depth, and water vapor contents for a given atmospheric profile and a specific aerosol model. If we assume the solar zenith angle and the water vapor content are the same for all pixels in the image, the only variable is aerosol optical depth.

MODTRAN [1] was used in this study. For each visibility value, MODTRAN was run three times with three surface reflectances ($r = 0{,}0.5,$ and 0.8), which enable us to determine three unknowns: L_p, S, and F. Thus, these three quantities depend on atmospheric visibility for the specific atmospheric profile, aerosol model, and solar illumination condition. If we know atmospheric visibility (equivalent to aerosol optical depth) or surface reflectance, we can determine the other from the TOA radiance.

Surface reflectance of the visible bands in clear regions are determined by the knowledge of minimum surface reflectance. This step may introduce uncertainty whose magnitude depends on the surface brightness. If there exist low-reflectance surfaces in a scene, such as vegetation, water, or wet soil, the error is very small. We quite often use a simpler approach. By assuming a visibility value for a clear region (e.g., 50 km), we can retrieve surface reflectance very accurately. We found from experiments that the uncertainty due to this assumption is reasonably small if the atmosphere is indeed quite clear.

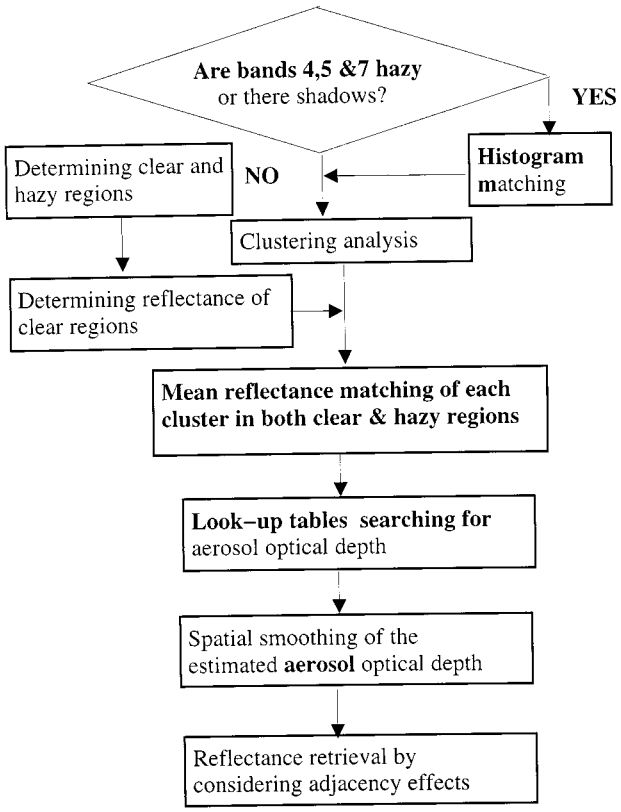

Fig. 1. Illustration of the procedure of the new atmospheric correction algorithm.

B. Estimation of Aerosol Optical Depth

This algorithm takes advantage of histogram matching algorithms [40]. However, instead of matching histograms of two regions (clear and hazy), we assume the average reflectance of each cover type to be the same under different atmospheric conditions (from clear to hazy). Thus, we can avoid the assumption that the landscape has the same percentage composition between the hazy and clear regions. Because bands 4, 5, and 7 imagery are much less contaminated by most aerosols, these three bands are used to classify all pixels into specific cover types. Mean reflectance matching is performed in the first three visible bands separately. A smoothing process is followed for each band to determine the final aerosol optical depth. The procedure is illustrated in Fig. 1. The major steps are discussed below in details.

If there are thick aerosols and thin clouds in the image, bands 4, 5, and 7 may be contaminated by scattering effects. A histogram matching process is first performed to adjust the values (reflectance, radiance or digital number) of these three bands. A clustering analysis using these three bands is then conducted. In our experiments, a K-mean clustering analysis has been extensively used, but other clustering algorithms can be easily employed. Specifying the number of clusters depends on the complexity of landscape. Ideally, the more complex the landscape, the larger number of clusters are needed. Our experiments indicated that 20–50 clusters produce similar results, probably because there are only three bands available for clustering analysis. More near-IR bands may improve the results.

It is assumed that there exist "clear regions" in a scene, which correspond to regions with the smallest aerosol loadings. There are several options in the current version of our code for separating clear regions from hazy regions. The first is to make use of the fourth component of the Tasseled Cap transformation [7], as used by other algorithms [40], [41]. This method often fails, particularly when the surfaces are very bright. The second is to determine hazy regions by segmenting the ratio of band 1 to band 4, which has been quite successful. The third is to draw the hazy regions by hand. Almost all image processing software packages have graphical interfaces that enable us to draw hazy regions conveniently. Of course, it is very time consuming for massive operational atmospheric correction tasks. Another major drawback of this method is that there is an obvious boundary effect along these manually drawn lines. Experiments demonstrate that combining ratio segmentation and hand drawing is very effective. The last option is to cluster the visible bands (bands 1, 2, and 3) since haze and thin clouds are very bright in the visible bands. But it is quite often that all bright surface objects are also included. A further cluster is performed to separate them since the brightness of hazes and thin clouds decrease with the increasing wavelength, but bright surfaces usually have the reverse trends.

Clouds often cast shadows over the clear regions. In the visible bands, shadows are not so obvious, but the near-IR bands (4, 5, and 7) can be significantly contaminated. The basic idea for removing these shadows is to classify cover types using the visible bands (1, 2, and 3) and to match their near-IR reflectance of the same cover types inside and outside the shadows. If there is no shadow in the scene or the shadow is under the cloud, this process can be omitted.

The next step is to match the average reflectance of each cluster between clear and hazy regions. Given surface reflectance, the aerosol optical depth (or visibility) of a hazy pixel can be determined by searching the look-up tables described in Section A.

Because aerosol optical depth is usually distributed more smoothly than that of surface reflectance, it might be possible that there are no corresponding clusters of hazy regions in the clear regions. In this case, a spatial low-pass filter is warranted. In our experiments, an average smoothing process works quite well. The typical window size is 5*5.

C. Surface Adjacency Effects

The adjacency effect is caused by complicated multiple scattering in the atmosphere-land surface system. The pixel values of high-resolution imagery over a heterogeneous landscape are affected by their neighboring pixels. As a result, dark pixels look brighter and bright pixels look darker. The practical implication to remotely sensed data is that imagery typically looks hazy and lack contrast. A pixel's value largely depends on its contrast with neighboring pixel values as the spatial resolution increases. This is particularly true if the atmosphere is not very clear. As the spatial resolution decreases, the mixture problem represents within-pixel effects. As the spatial resolution increases, the adjacency problems represents between-pixel effects. The mixture problem has been extensively investigated (e.g., [5], [19], and [30]), but adjacency effects deserve continuing investigation as we are increasingly faced with greater amounts of high-resolution satellite imagery.

Earlier studies on the adjacency effect are summarized by an excellent review [21], and few studies have reported successful results in removing adjacency effects since then. All studies can be grouped into two broad categories: 1) using the atmospheric point spread function (PSF) and 2) developing empirical formulae. Different methods have been explored to calculate the atmospheric PSF, including Monte-Carlo simulations [34], [36], [39], and radiosity simulation [2].

The adjacency effect can be corrected by using the Fourier-transform approach given the atmospheric PSF [20], [25], [31], [32]. Although efforts have been made to develop empirical function of the atmospheric modulation transfer function (MTF) that is the Fourier transform (FT) of the atmospheric PSF, most methods for calculating the atmospheric PSF/MTF are computationally expensive. The validity of the atmospheric PSF method for correcting the adjacency effect in high-resolution satellite imagery is also still questionable. When the atmosphere is turbid and multiple scattering dominates, or where the surface reflects strongly, there are multiple interactions between the atmosphere and the surface. Thus, upwelling radiance is not simply a convolution of the atmospheric PSF with the surface reflectance. As we will demonstrate later, the adjacency effect is significant only when the multiple interaction between the atmosphere and a heterogeneous surface is dominant.

Actually this is a typical three-dimensional (3-D) radiative transfer problem [10]. Theoretically, we should be able to calculate adjacency effects by solving 3-D radiative transfer equation. Unfortunately, solving a 3-D radiative transfer equation is computationally expensive. For operational applications, empirical solutions are more appealing. For TM imagery, Kaufman [20] developed a simple formula of the normalized atmospheric modulation transfer function (MTF) with the relative accuracy of 25 percent compared with a Monte Carlo simulation results. To apply that equation to correct the adjacency effects, a Fourier transformation is needed.

Tanre *et al.* [46] derived a TOA reflectance formula by defining an effective reflectance of a neighborhood and incorporated it into the 6S code [50]. But the interpretation of the effective reflectance in this formulation is not straightforward.

Takashima and Masuda [47] developed a formula with nine terms, which has been incorporated into the ASTER atmospheric correction algorithm [49]. When the formula is very complicated, however, the inversion of surface reflectance may become more difficult.

In this study, we address the surface adjacency effects for the nadir-viewing sensors (e.g., ETM+ located at the top of the atmosphere above a Lambertian surface. We try to define an "effective " surface reflectance so that the classic plane-parallel formulae can be exactly applied. If the surface is not homogeneous, the plane-parallel formula is not valid. This is a typical 3-D radiative transfer problem. Our purpose is to develop an empirical formula for calculating the "effective" reflectance of a heterogeneous Lambertian surface so that the exact formula (1) is valid for a heterogeneous surface except that the reflectance r is replaced by the "effective reflectance" r_e. The basic approach we employed was to run the 3-D radiative transfer code (SHDOM) [10] over a step-function surface and fit an empirical formula of "effective" reflectance.

The SHDOM has been discussed by Evans [10] in detail. In the course of solving the 3-D radiative transfer equation, SHDOM transforms between the discrete ordinate and spherical harmonic representations. It handles the 3-D variations of both atmosphere and surface. Surface directional reflectance can be also specified. This has been used in various applications [4], [11], [27].

Based on our exploratory simulations with different aerosol scaling heights, solar zenith angles, and aerosol optical depth, it is found that the aerosol optical depth is the dominating factor. We also found that Rayleigh scattering causes the secondary order of the adjacency effects, which is consistent with the earlier studies (e.g., [39], [34]). Therefore, we designed our numerical simulations with different aerosol optical depths over a step-function surface (two-dimensional [2-D] radiative transfer). The surface reflectances were set 0.05 for dense vegetation or water and 0.8 for snow or bright sand. The atmosphere was stratified with aerosol scattering coefficient b_a decreasing exponentially with altitude z with a scale height H_a[15]

$$b_a = b_0 \exp\left(\frac{-z}{H_a}\right) \tag{2}$$

where b_0 is the aerosol scattering coefficient at the surface. SHDOM code was run over a H_0 (7-km) slab of the atmos-

phere. Assuming no absorption, the aerosol optical depth is given by

$$\tau = b_0 H_a \left[1 - \exp\left(\frac{-H_0}{H_a}\right)\right]. \tag{3}$$

H_a was set 1 km as suggested by Gordon and Castano [15]. Six aerosol optical depths were used: 0.05, 0.3, 0.6, 0.9, 1.2, and 1.5. SHDOM code was run over three solar zenith angles: 10°, 30°, and 50°. For each case, atmospheric parameters such as L_p, S, and F in (1) were derived by running the plane-parallel mode of the SHDOM code with two surface reflectances 0.0 and 0.5. We defined an empirical weighting function $g(s)$ whose convolution with the step-function produces the "effective" reflectance

$$r_e = \frac{\int g(s) r(s) ds}{\int g(s) ds} \tag{4}$$

where $r(s)$ is the true step-function surface reflectance and s is the distance from the central location that can be used as the radial distance in the fitted empirical function below. The fitted empirical function is

$$g(s) = f_1(\tau)\exp(-1.424s) + f_2(\tau)\exp(-12\,916s) \tag{5}$$

where s is the radial distance from the central pixel (km), τ is the aerosol optical depth, and

$$f_1(\tau) = 0.003\tau \tag{6}$$

$$f_2(\tau) = 0.071\tau^3 - 0.061\tau^2 - 0.439\tau + 0.996. \tag{7}$$

Note that these formulae are general and suitable for all the spectral bands. Because the aerosol optical depths decrease as wavelength, the adjacency effects are the largest in the shorter wavelength and decrease at the longer wavelength.

It is evident that the first term of the right side of (5) represents the contribution from the background pixels, the second term represents the contribution from the current pixel and its nearest neighboring pixels. In the literature, the second term is often represented by a delta function. The normalized functions are illustrated in Fig. 2. We can see that the background contribution largely depends on the aerosol optical depth. If the optical depth is small (i.e., atmosphere is very clear), the major contribution of the pixel value is from the pixel itself. As the aerosol optical depth increases, the background contribution (i.e., adjacency effects) becomes larger.

To illustrate how effective this approximate formula is, we present the results of a numerical experiment in Fig. 3. SHDOM was used to calculate downward and upwelling fluxes at the 2-D Lambertian surface with three aerosol optical depths. The calculated "effective" reflectances (ratio of the upwelling and downward fluxes) are represented as dots in Fig. 3. The predicted surface "effective" reflectances using (5) are shown in the solid lines in Fig. 3 It is clear that formula (5) captures the surface adjacency effect very well.

It is believed that the fitted empirical weighting function (5) from a 2-D step-function surfaces is also suitable for the 3-D domain (e.g., an image). The "effective" reflectance of the satellite imagery can be calculated in the discrete form

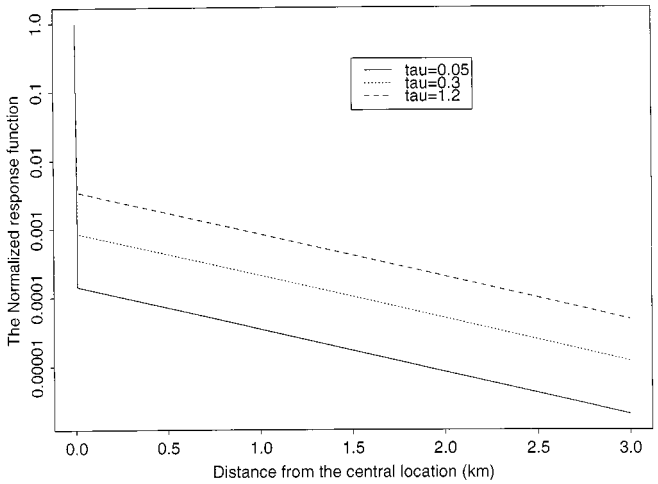

Fig. 2. Relative contributions of the neighboring pixels from (5).

$$r_e = \frac{\sum_i^N \sum_j^N r_{ij} g_{ij}}{\sum_i^N \sum_j^N g_{ij}} \tag{8}$$

where g_{ij} is the relative contribution from the pixel (i,j) and can be integrated from (5) over pixel (i,j)

$$g_{ij} = \int_{x_i}\int_{y_j} g\left(\sqrt{x^2+y^2}\right) dxdy. \tag{9}$$

N is the window size in which all pixels make contributions to the apparent value of the central pixel and can be determined by a threshold value α

$$\alpha = \frac{\sum_i^N \sum_j^N g_{ij}}{\sum_i^\infty \sum_j^\infty g_{ij}}. \tag{10}$$

Fig. 4 illustrates the dependence of the window size N on the pixel size and the aerosol optical depth. Note that the aerosol optical depth is generally defined and not associated with a specific spectral band. Generally speaking, when the aerosol optical depth is smaller, the window size can be smaller.

To examine whether the formula derived from 2-D step-function surface is valid for a 3-D image, we extracted several 30×30 pixel windows from ETM+ band 1 imagery acquired on July 28, 1999, at Beltsville, MD. After running SHDOM for three optical depths (0.3, 0.6, 0.9), we compared them with the plane-parallel version with the effective reflectance. In many cases where reflectance in the window is quite homogeneous, the three results are quite similar. When reflectances in the window vary dramatically, the differences are very large. One example is shown in Fig. 5, where all pixels were extracted from a window in which there are concrete houses and vegetation canopies. The weighing window is 12×12. A total of 36 pixels in the center of the window are compared among three methods. The one-dimensional (1-D) method in the figure represents the plane-parallel formula with an average (mean) reflectance of the window. The new 1-D method is the one we proposed using a weighted average. In this case, the plane-parallel method

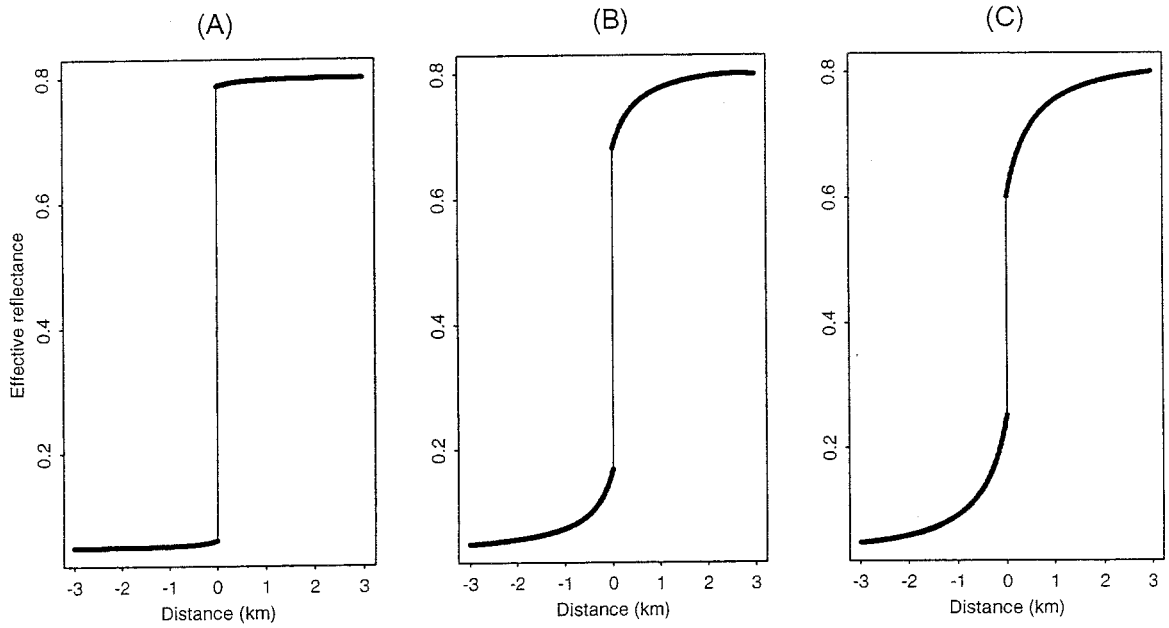

Fig. 3. Fitting the "effective" reflectance using the empirical model under three aerosol optical depths (a) 0.05, (b) 0.6, and (c) 1.2.

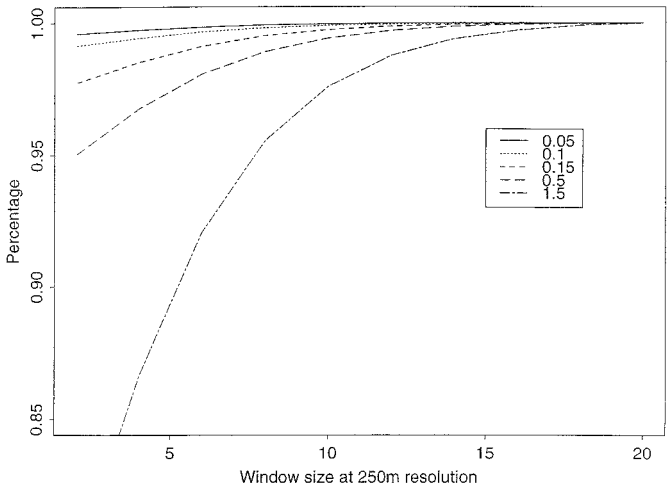

Fig. 4. Effects of different window sizes.

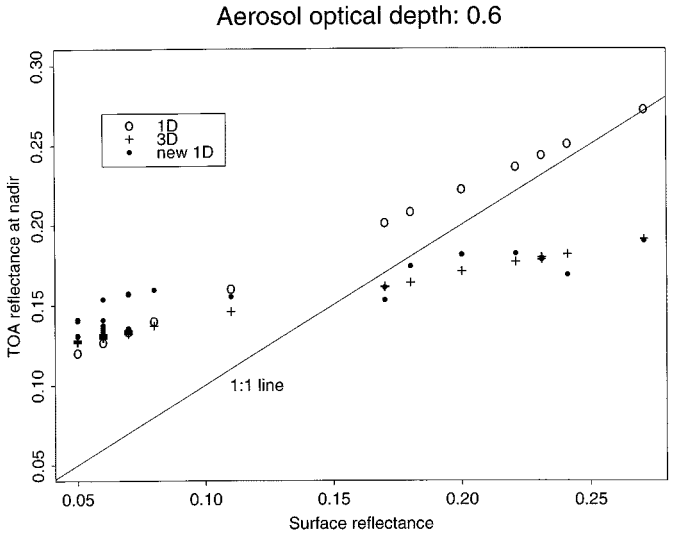

Fig. 5. Testing the empirical formula of the "effective"reflectance using real ETM+ band 1 image.

overestimates high reflectance significantly. Because of the adjacency effects, the bright pixels (houses) tend to be darker. The new approximate formula produces the points very close to the 3-D simulation results.

Note that the fitted empirical function (5) is rotationally symmetric, which may not be valid for a non-Lambertian surface and/or the case that the viewing zenith angle is not at nadir.

D. Surface Reflectance Retrieval

After estimating the aerosol optical depth, the retrieval of surface reflectance is straightforward. We simply to solve equation (1) where all quantities related to the atmospheric conditions are determined by searching the look-up tables. The retrieved surface reflectance is actually the effective reflectance. The real reflectance of each pixel can be determined from (8). Theoretically, it has to be an iterative procedure since r_{ij} must be real reflectance, but our preliminary results indicate no need for iterations because there will be generally very small improvements under most circumstances.

E. Variant Version for Spatial Normalization

For certain applications (e.g., land cover and land use mapping), it may not be necessary to derive surface reflectance. The TOA radiance is fine as long as the atmospheric condition over the whole image is uniform. When the aerosol distribution is not homogeneous, this new atmospheric correction algorithm can be used to normalize the image spatially. The basic procedure is very similar to what is just described above. The whole procedure roughly consists of five steps. First, an option is used to determine the hazy regions. Second, the near-IR bands are used to identify different cover types using a clustering analysis. Third, the mean value of the clear pixels of the same cluster is used to

Fig. 6. Atmospheric correction examples of three scenes (Bands 1, 2, and 3). The first row shows the true color composite images before atmospheric correction, and the second row after atmospheric correction.

represent the value of the hazy pixels. Fourth, the difference of the original image and the newly calculated radiance values is calculated and spatially smoothed. Lastly, the original radiances are subtracted from the smoothed values to form the normalized pixel value of the hazy regions. The final image values are still in radiance, but heterogeneous aerosol effects have been removed. If the original pixels values are the digital numbers, the procedure is the same. Since the final value is not surface reflectance, we denote this procedure as a spatial normalization method.

IV. Correction Examples

Fig. 6 compares three true color composite imagery before and after atmospheric correction using this method. These are three 600×600 windows from the same ETM+ imagery acquired on November 17, 1999, but they have different surface reflectance and aerosol distribution patterns. The solar zenith angle is 63.51° and azimuth angle is 162.83°. The atmospheric effects are much larger in these blue band images. In these examples, the ratios of band 1 to band 4 images were segmented to generate clear/hazy regions. From these figures, we can see that atmospheric correction produces significantly different visual effects. Most of the hazy regions have been cleaned up. Note that all pixels seem brighter after atmospheric correction. The reason is that the dynamic range of pixel values becomes smaller after atmospheric correction, but the display brightness range is the same.

It is important to point out that the dark-object method fails to correct these three images since no dense vegetation canopies are widely distributed over the agricultural region in the winter season. Use of the histogram matching algorithm is also inappropriate since landscape of the hazy and clear areas are not exactly the same and the spatial distribution of aerosol optical depth changes dramatically.

In the companion paper, we will quantitatively evaluate the accuracy of this atmospheric correction algorithm over the EOS Land Core Validation Site, Beltsville, MD. The improvements to different applications after atmospheric correction will also be demonstrated.

V. A Brief Summary

We present a new atmospheric correction algorithm to retrieve surface reflectance from Landsat7 ETM+ imagery. The innovative part of this algorithm is to account for heterogeneous aerosol scattering effects in a scene and to correct the surface adjacency effects using a simple analytical formula.

The basic idea is to identify surface clusters using bands 4, 5, and 7 that are less contaminated by aerosols. The average reflectance of each cluster in both clear and hazy regions is matched, which allows us to determine the aerosol optical depth. A low-pass smoothing process is performed to determine the distribution of aerosol optical depth in each band. Surface reflectance is finally determined by searching the look-up tables.

Note that we did not consider the adjacency effects of the aerosol horizontal variations. When the sun is not at zenith, the aerosol optical depths of the neighboring pixels along the solar path affect the current pixel values. However, the spatial variation of the aerosol optical depth is very smooth. The adjacency effect is actually compressed in the step of estimating aerosol optical depth since it provides us with the "equivalent" optical depth of the current pixel. Our sensitivity study showed that this error is smaller than the uncertainty of the aerosol optical depth estimation.

A few correction examples are given to demonstrate that this algorithm is very effective for retrieving surface reflectance for different aerosol and surface distribution patterns. A quantitative evaluation of the correction accuracy will be given in the companion paper.

A variant version of this algorithm that normalizes the image spatially is also discussed. The final value from this procedure is not surface reflectance, but it can remove the heterogeneous aerosol effects in the same way.

This algorithm is very general and can be used for any atmospheric and surface conditions, and is therefore suitable for most operational applications. Although this algorithm assumes a Lambertian surface and availability of other ancillary information about aerosol phase function, water vapor, ozone, etc., it does not make any other fundamental assumptions. Thus, it can potentially be extended to other sensors, such as ASTER on the Terra spacecraft and ALI (advanced land imager) on the Earth Observer-1 Satellite. Research along this line is under way.

ACKNOWLEDGMENT

The authors are very grateful to Dr. F. Evans for providing the SHDOM code and for valuable discussions of the simulation results, Dr. C. Huang for providing the ETM+ imagery used in this paper, Mr. C. Shuey for preparing for this manuscript, and particularly two anonymous reviewers for providing valuable comments that have greatly improved this paper.

REFERENCES

[1] A. Berk, L. S. Bernstein, G. P. Anderson, P. K. Acharya, D. C. Robertson, J. H. Chetwynd, and S. M. Adler-Golden, "MODTRAN cloud and multiple scattering upgrades with application to AVIRIS," *Remote Sens. Environ.*, vol. 65, pp. 367–375, Sept. 1998.

[2] C. C. Borel and S. A. W. Gerstl, "Adjacency-blurring-effect of scenes modeled by the radiosity method," in *Proc. SPIE*, vol. 1688, 1992, pp. 620–624.

[3] M. T. Chahine, H. Aumann, M. Goldberg, L. McMillin, P. Rosenkranz, D. Staelin, L. Strow, J. Susskind, and M. Gunson, "AIRS-Team Retrieval for Core Products and Geophysical Parameters, Level 2 A Algorithm Theoretical Basis Document, 2.1," NASA, Washington, DC, 1999.

[4] L. H. Chambers, B. A. Wielicki, and K. F. Evans, "Accuracy of the independent pixel approximation for satellite estimates of oceanic boundary layer cloud optical depth," *J. Geophys. Res.*, vol. 102, no. D2, pp. 1779–1794, Jan. 1997.

[5] C. I. Chang and H. Ren, "An experiment-based quantitative and comparative analysis of target detection and image classification algorithms for hyperspectral imagery," *IEEE Trans. Geosci. Remote Sensing*, vol. 38, pp. 1044–1063, Mar. 2000.

[6] P. Chavez Jr, "Image-based atmospheric corrections — Revisited and improved," *Photogramm. Eng. Remote Sensing*, vol. 62, pp. 1025–1036, Sept. 1996.

[7] E. P. Crist and R. C. Cicone, "A physically-based transformation of Thematic Mapper data — The tasseled cap," *IEEE Trans. Geosci. Remote Sensing*, vol. GE-22, pp. 256–263, May 1984.

[8] H. R. Gordon and D. J. Castano, "Aerosol analysis with the Coastal Zone Color Scanner: a simple method for including multiple scattering effects," *Appl. Opt*, vol. 28, pp. 1320–1326, Apr. 1989.

[9] S. N. Goward and D. L. Williams, "Landsat and earth systems science: Development of terrestrial monitoring," *Photogramm. Eng. Remote Sensing*, vol. 63, pp. 887–900, July 1997.

[10] K. F. Evans, "The spherical harmonics discrete ordinate method for three-dimensional atmospheric radiative transfer," *J. Atmos. Sci.*, vol. 55, pp. 429–464, 1998.

[11] K. F. Evans, A. H. Evans, I. G. Nolt, and B. T. Marshall, "The prospect for remote sensing of cirrus clouds with a submillimeter-wave spectrometer," *J. Appl. Meteorol.*, vol. 38, pp. 514–525, May 1999.

[12] R. S. Fraser and Y. J. Kaufman, "The relative importance of scattering and absorption in remote sensing," *IEEE Trans. Geosci. Remote Sensing*, vol. GE-18, pp. 2577–2584, 1985.

[13] R. S. Fraser, R. A. Ferrare, Y. J. Kaufman, B. L. Markham, and S. Mattoo, "Algorithm for atmospheric corrections of aircraft and satellite imagery," *Int. J. Remote Sensing*, vol. 13, pp. 541–557, 1992.

[14] B. Gao and Y. kaufman, "The MODIS Near-IR Water Vapor Algorithm," NASA EOS ATBD: MOD05. 25pp, NASA, Washington, DC, 1998.

[15] H. R. Gordon and D. J. Castano, "Aerosol analysis with the Coastal Zone Color Scanner: A simple method for including multiple scattering effects," *Appl. Opt.*, vol. 28, pp. 1320–1326, Apr. 1989.

[16] S. N. Goward and D. L. Williams, "Landsat and earth systems science: Development of terrestrial monitoring," *Photogramm. Eng. Remote Sensing*, vol. 63, pp. 887–900, July 1997.

[17] F. G. Hall, D. E. Strebel, J. E. Nickeson, and S. J. Goetz, "Radiometric rectification: Toward a common radiometric response among multidate, multisensor images," *Remote Sens. Environ.*, vol. 35, pp. 11–27, 1991.

[18] M. Hess, P. Koepke, and I. Schult, "Optical properties of aerosols and clouds: The software package OPAC," *Bull. Amer. Meteorol. Soc.*, vol. 79, pp. 831–844, May 1998.

[19] Y. H. Hu, H. B. Lee, and F. L. Scarpace, "Optimal linear spectral unmixing," *IEEE Trans. Geosci. Remote Sensing*, pt. Part 2, vol. 37, pp. 639–644, Jan. 1999.

[20] Y. J. Kaufman, "Atmospheric effect on spatial resolution of surface imagery: Errata," *Appl. Opt.*, vol. 23, pp. 4164–4172, 1984.

[21] ——, "The atmospheric effect on remote sensing and its correction," in *Theory and Applications of Optical Remote Sensing*, G. Asrar, Ed. New York: Wiley, 1989.

[22] Y. J. Kaufman and C. Sendra, "Automatic atmospheric correction," *Int. J. Remote Sensing*, vol. 9, pp. 1357–1381, 1988.

[23] Y. J. Kaufman, A. Karnieli, and D. Tanre, "Detection of dust over deserts using satellite data in the solar wavelengths," *IEEE Trans. Geosci. Remote Sensing*, vol. 38, pp. 525–531, Jan. 2000.

[24] Y. J. Kaufman, A. Wald, L. A. Lorraine, B. C. Gao, R. R. Li, and L. Flynn, "Remote sensing of aerosol over the continents with the aid of a 2.2 μm channel," *IEEE Trans. Geosci. Remote Sensing*, vol. 35, pp. 1286–1298, July 1997.

[25] V. V. Kozoderv, "Correction of space image for atmospheric effects," *Sov. Int. J. Remote Sensing*, vol. 3, pp. 255–271, 1995.

[26] J. Lavreau, "De-hazing Landsat Thematic Mapper images," *Photogramm. Eng. Remote Sensing*, vol. 57, pp. 1297–1302, 1991.

[27] S. Liang, "Numerical experiments on spatial scaling of land surface albedo and leaf area index," *Remote Sens. Rev.*, vol. 19, pp. 225–242, 2000.

[28] S. Liang, H. Fallah-Adl, S. Kalluri, J. JaJa, Y. Kaufman, and J. Townshend, "Development of an operational atmospheric correction algorithm for TM imagery," *J. Geophys. Res.*, vol. 102, pp. 17 173–17 186, 1997.

[29] K. N. Liou, *An Introduction to Atmospheric Radiation*. New York: Academic, 1980.

[30] F. Maselli, "Multiclass spectral decomposition of remotely sensed scenes by selective pixel unmixing," *IEEE Trans. Geosci. Remote Sensing*, pt. Part 2, vol. 36, pp. 1809–1820, Sept. 1998.

[31] Y. Mekler and Y. J. Kaufman, "The effect of earth's atmosphere on contrast reduction for a uniform surface albedo and 'two-halves' field," *J. Geophys. Res.*, vol. 85, pp. 4067–4083, 1980.

[32] ——, "Contrast reduction by the atmosphere and retrieval of nonuniform surface reflectance," *Appl. Opt.*, vol. 21, pp. 310–316, 1982.

[33] P. Menzel and L. Gumley, *MODIS Atmospheric Profile Retrieval ATBD*, Version 3 ed. Washington, DC: NASA, 1996.

[34] C. Miesch, X. Briottet, Y. H. Kerr, and F. Cabot, "Monte Carlo approach for solving the radiative transfer equation over mountainous and heterogeneous areas," *Appl. Opt.*, vol. 38, pp. 7419–7430, 1999.

[35] S. Moran, R. D. Jackson, P. N. Slater, and P. M. Teillet, "Evaluation of simplified procedures for retrieval of land surface reflectance factors from satellite sensor output," *Remote Sens. Environ.*, vol. 41, pp. 169–184, 1992.
[36] W. A. Pearce, "A Study of the Effects of the Atmosphere on Thematic Mapper Observations," Tech. Rep. 004–77, EG@G, Washington Anal. Service Center, Riverdale, MD, 1977.
[37] T. Popp, "Correcting atmospheric masking to retrieve the spectral albedo of land surface from satellite measurements," *Int. J. Remote Sensing*, vol. 16, pp. 3483–3508, 1995.
[38] J. F. Porter, "The channel correlation method for estimating aerosol levels from multispectral scanner data," *Photogramm. Eng. Remote Sensing*, vol. 50, pp. 43–52, 1984.
[39] P. N. Reinersman and K. L. Carder, "Monte Carlo simulation of the atmospheric point-spread function with an application to correction for the adjacency effect," *Appl. Opt.*, vol. 34, pp. 4453–4471, 1995.
[40] R. Richter, "A spatially adaptive fast atmospheric correction algorithm," *Int. J Remote Sens.*, vol. 17, pp. 1201–1214, 1996.
[41] ——, "Atmospheric correction of satellite data with haze removal including a haze/clear transition region," *Comput. Geosci.*, vol. 22, pp. 675–681, 1996.
[42] R. Santer, V. Carrere, P. Dubuisson, and J. C. Roger, "Atmospheric correction over land for MERIS," *Int. J. Remote Sensing*, vol. 20, pp. 1819–1840, 1999.
[43] P. Switzer, W. Kowalik, and R. J. P. Lyon, "Estimation of atmospheric path-radiance by the covariance matrix method," *Photogramm. Eng. Remote Sensing*, vol. 47, pp. 1469–1476, 1981.
[44] D. Tanre and M. Legrand, "On the satellite retrieval of Saharan dust optical thickness over land: two different approaches," *J. Geophys. Res.*, vol. 96, pp. 5221–5227, Mar. 1991.
[45] D. Tanre, P. Y. Deschamps, C. Devaux, and M. Herman, "Estimation of Saharan aerosol optical thickness from blurring effects in Thematic Mapper data," *J. Geophys. Res.*, vol. 93, pp. 15 955–15 964, Dec. 1988.
[46] D. Tanre, M. Herman, and P. Y. Deschamps, "Influence of the background contribution upon space measurements of ground reflectance ," *Appl. Opt.*, vol. 20, pp. 3673–3684, 1981.
[47] T. Takashima and K. Masuda, "Operational procedure of atmospheric correction on satellite visible data allowing for the adjacency effect," in *Proc. SPIE*, vol. 2817, 1996, pp. 70–81.
[48] P. M. Teillet and G. Fedosejevs, "On the dark target approach to atmospheric correction of remotely sensed data," *Can. J. Remote Sensing*, vol. 21, pp. 374–387, 1995.
[49] K. Thome, F. Palluconi, T. Takashima, and K. Masuda, "Atmospheric correction of ASTER," *IEEE Trans. Geosci. Remote Sensing*, vol. 36, pp. 1199–1211, July 1998.
[50] E. Vermote, D. Tanre, J. L. Deuze, M. Herman, and J. J. Morcrette, "Second simulation of the satellite signal in the solar spectrum: An overview," *IEEE Trans. Geosci. Remote Sensing*, vol. 35, pp. 675–686, May 1997.

Shunlin Liang (M'94–SM'01) received the Ph.D. degree in remote sensing and GIS from Boston University, Boston, MA.

He was a Postdoctoral Research Associate at Boston University from 1992 to 1993, and Validation Scientist of the NOAA/NASA Pathfinder AVHRR Land Project from 1993 to 1994. He is currently an Associate Professor with the University of Maryland, College Park. His present research interests focus on land surface data assimilation, parameter retrieval from remotely sensed data, and spatial analysis. He chaired various sessions of the international conferences and served as the chairman of the IEEE Geosciences and Remote Sensing Society, Washington/North Virginia Chapter (2000). He is currently the Principal Investigator of the NASA EOS Terra Validation Team, NASA Earth Observer-1 Science Team, and the International ALOS, CHRIS/PROBA, and POLDER Science Working Teams.

Dr. Liang organized the International Forum on BRDF, San Francisco, CA, in December 1998, and co-edited a special issue of the Remote Sensing Reviews. He is an associate editor of the IEEE TRANSACTIONS ON GEOSCIENCE AND REMOTE SENSING.

Hongliang Fang received the B.S. degree in geography from East China Normal University, Shanghai, in 1993, and the M.S. degree in cartography and GIS from the Institute of Geography, Chinese Academy of Sciences, Beijing, in 1996. He is currently pursuing the Ph.D. degree at the University of Maryland, College Park.

His previous interest was on use of remote sensing and GIS in a variety of fields such as environment monitoring, land cover/use, biomass monitoring, and wetland ecology. His most recent interest is in retrieving land surface parameters from remotely sensed data.

Mingzhen Chen received the Ph.D degree in remote sensing of soils from Zhejiang Agricultural University, Zhejiang, China.

He was an Associate Professor with Zhejiang University from 1996 to 1998. He is currently a Visiting Research Scientist at the University of Maryland, College Park. His research interests focus on remote sensing and GIS applications such as retrieving land surface parameters from remotely sensed data, land cover and land use, biomass, and environment monitoring.